

Article

Study of Microstructure, Crystallographic Phases and Setting Time Evolution over Time of Portland Cement, Coarse Silica Fume, and Limestone (PC-SF-LS) Ternary Portland Cements

Esperanza Menéndez ¹, Miguel Ángel Sanjuán ²  and Hairon Recino ^{1,*} 

¹ Eduardo Torroja Institute for Construction Science, Spanish National Research Council, CSIC C/Serrano Galvache, 4, 28033 Madrid, Spain; emm@ietcc.csic.es

² Spanish Institute of Cement and its Applications (IECA), C/José Abascal, 53, 28003 Madrid, Spain; masanjuan@ieca.es

* Correspondence: h.recino@ietcc.csic.es; Tel.: +34-911035763

Abstract: The use of silica fume as a partial replacement for Ordinary Portland Cement provides a wide variety of benefits, such as reduced pressure on natural resources, reduced CO₂ footprint, and improved mechanical and durability properties. The formation of more stable crystallographic phases in the hardened cement paste can promote resistance to concrete attacks. However, using coarse silica fume may result in lower expenses and shorter workdays. In this work, coarse silica fume was used as a partial replacement of cement, by weight, at 3%, 5%, and 7%, and it was used as limestone filler at different particle sizes. The size of coarse silica fume used was 238 μm. The microstructural, compositional analysis, and crystalline phase content of mixed cements at different ages were evaluated. The addition of coarse silica fume and limestone promoted pore refinement of the composites and increased the calcium and silica content. The filling effect of fine limestone and coarse silica fume particles, as well as the formation of CSH gel, was found to be the main reason for the densified microstructure. The contributions of combined coarse silica fume and limestone improve the stability of CSH gels and pozzolanic reaction.

Keywords: ternary cements; coarse silica fume; limestone; crystallography phases; properties of cementitious materials; microstructural analysis



Citation: Menéndez, E.; Sanjuán, M.Á.; Recino, H. Study of Microstructure, Crystallographic Phases and Setting Time Evolution over Time of Portland Cement, Coarse Silica Fume, and Limestone (PC-SF-LS) Ternary Portland Cements. *Crystals* **2023**, *13*, 1289. <https://doi.org/10.3390/cryst13081289>

Academic Editors: Nima Farzadnia, Bin Ma, Heeyoung Lee and Xu Gao

Received: 25 July 2023

Revised: 11 August 2023

Accepted: 16 August 2023

Published: 21 August 2023



Copyright: © 2023 by the authors. Licensee MDPI, Basel, Switzerland. This article is an open access article distributed under the terms and conditions of the Creative Commons Attribution (CC BY) license (<https://creativecommons.org/licenses/by/4.0/>).

1. Introduction

Lowering the carbon dioxide content associated with Portland cement production is currently a major concern worldwide. For instance, the European Union is committed to a target of a 55% reduction in greenhouse gas emissions by 2030 compared to 1990 levels [1]. Nowadays, carbon neutrality is the main challenge that European industries are facing [2]. In particular, the Portland cement industry is dealing with its decarbonization and modernization [3]. The use of high amounts of cement constituents, other than clinker, as a partial replacement for Portland clinker contributes to the reduction of carbon dioxide emissions and the environmental impact of the Portland cement production. In an effort to produce low-carbon footprint and cost-effective cements, many new formulations are currently being investigated.

Recently, Frías et al. [4] studied ternary cements, made with common Portland cement or calcium sulfoaluminate cement, and three kinds of Construction and Demolition Wastes (fines from recycled concrete aggregates, glass powder, and gypsum). Analyzing their physical and mechanical characteristics, they concluded that these new mixes comply with the specifications of the current Portland cement standards [5]. Zeraoui et al. [6] prepared some ternary binders by mixing common Portland cement, ground granulated blast-furnace slag, and flash-calcined sediment. They found that the mix with 10% flash-calcined sediment and 40% ground granulated blast-furnace slag could replace 50% common Portland cement.

In particular, the flash-calcined sediment presents a high-water demand, which reduces the mortar's workability. By contrast, it promotes the mortar's compactness and density. Pinheiro et al. [7] assessed a ternary cement made with 23% calcined clay, 2% nanosilica, and common Portland Cement. They reported that the transformation of macropores into mesopores lead to a reduction in the global porosity.

Papatzani and Paine [8] studied Portland cement–limestone–fly ash formulations, which were further optimized with the addition of silica fume (5% and 10% by mass). The 10% silica fume addition was excessive, and some unreacted particles were found by SEM observations. Li et al. [9] used silica fume, fly ash, and limestone powder to produce Ultra-High-Performance Concrete. They developed a multi-component model, based on the pozzolanic reactions, to quantify the heat released during the hydration reaction. As expected, silica fume significantly improved the compressive strength of concrete, whereas fly ash was better than limestone powder in terms of 28 day compressive strength gain. Zhao et al. [10] investigated the improvement of the packing density of ternary cement pastes made with ground slag and silica fume. The enhanced packing density and the decrease in the water film thickness through the filling effect leads to an increase in fluidity and 28 day compressive strength.

Srinivas et al. [11] manufactured ternary cements by mixing Portland cement, coal fly ash, and silica fume or limestone powder to assess their rheological properties, and they found that their enhanced buildability was linked to their static yield stress. Therefore, silica fume and limestone, ranging from 5% to 10% with higher static yield stress, enhanced the buildability and reduced the anisotropic mechanical properties. Surprisingly, the compressive strength was lower (about 2–7%) for the specimens containing silica fume compared to the control specimen. Furthermore, the compressive strength was higher (about 1–4%) for the specimens containing 10% and 5% limestone powder, respectively.

Kang et al. [12] reported high compressive strength achievements (about 200 MPa) by mixing silica fume with Portland limestone cement in Ultra High-Performance Fiber-Reinforced Concrete. Furthermore, Li et al. [13] found a positive plasticization effect when Limestone I was used in Ultra High-Performance Concrete made with silica fume. Apparently, the pozzolanic reaction was more intensive than calcium silicate (C_3S and C_2S) hydration. Accordingly, the strength development at later ages was improved as a result of the denser concrete matrix. They concluded that 50% volume of the limestone powder is the optimal content for Ultra High-Performance Concrete.

Ternary cements produced with clinker, limestone powder, and a third constituent, such as coarse silica fume, could be a promising option due to the good availability of the constituents and the low environmental impact.

Currently, silica fume is the most widely utilized type of ultrafine particles, notwithstanding their higher price, for quality reasons. Early research studies on the optimization of packing density were based on the use of ultrafine particles [14,15]. It has been widely agreed upon that silica fume provides nucleation sites for C–S–H gel, accelerates the Portland cement hydration, and provides silicon oxide for the pozzolanic reaction, at later ages, by consuming Portlandite and producing additional C–S–H gel with a lower Ca/Si ratio [16,17]. Silicate ions are generated in two possible ways: (i) $Si(OH)_4$ deprotonation, leading to $H_3SiO_4^-$ (when $pH > 9$), and (ii) silica dissolution when $pH > 10.7$, leading to $H_3SiO_4^-$ [16]. The beneficial contributions of silica in cement-based materials are twofold. Firstly, new C–S–H gel is formed in the so-called pozzolanic reaction with calcium oxide (portlandite), which results from the hydration of alite and belite. Secondly, a filler effect proceeds when some particles partially fill the capillary pores, leading to a denser microstructure. In addition, C–S–H gel could nucleate on the silica surface (seeding effect) [17].

The ground limestone is being widely utilized worldwide in common Portland cements. This well-known cement constituent affects their properties by dilution, filler, nucleation, and chemical effects; such characteristics depends on the limestone particle size distribution (PSD) and its percentage in the cement. Accordingly, fine limestone accelerates

the Portland cement hydration at early ages due to the reduction of the activation energy of the mentioned reaction. In addition, it promotes the dissolution of the Portland cement and its additions [18]. Instead, this effect will be less pronounced in coarse limestone [19]. Furthermore, packing density can increase at low limestone levels (<10–15%) [20] and reduce the setting time. Quantum leaps of the packing density have also been reported with limestone contents from 5 to 35% [21].

The aluminum ions present in the cement (mainly C₃A) can react with the calcium carbonate (limestone) in portlandite saturation conditions, generating hemicarboaluminate, which can be converted into monocarboaluminate at late ages [22]. Dhandapani et al. [22] found that carboaluminate formation is not the main reason for property enhancement in ternary cements containing limestone. Furthermore, they highlighted that limestone changes the hydration kinetics of cements at early ages in a different manner depending on the nature, particle size distribution, and limestone content.

From there, this paper covers the microstructural characteristics of clinker–limestone–silica fume ternary cements. It deals with the silica fume and limestone effects on mortar.

2. Materials and Methods

Portland cement (PC), coarse silica fume (SF), and limestone (LS) were used as raw materials to prepare ternary cements. Portland cement of grade 42.5 (CEM I 42.5 R, according to the European standard EN 197-1 [23]) and the limestone were obtained from LafargeHolcim España Cement Co., Villaluenga de la Sagra, Toledo, Spain. Ferroatlántica, Sada, Spain provided a coarse silica fume (SiO₂). Their chemical is given in Table 1. Table 2 shows the cementitious mix formulations using these raw materials. Codification criteria are used as follows:

- Ref: Sample composed of 100% CEM I 42.5 R cement type (used as test reference).
- H: Corresponds to the percentage of silica fume substitution by weight of the cement.
- LX1-X2-X3: The amounts of limestone retained are represented by the replacement percentages by weight of the cement, where X1 is the fraction with 10% retained, X2 is the fraction with 20% retained, and X3 is the fraction with 50% retained.

Table 1. Chemical composition of raw materials: coarse silica fume, limestone, and cement (%).

Chemical Composition (%)	Cement	Coarsesilica Fume	Limestone	Physical Properties of Cement	
SiO ₂	20.0	96.1	3.4	Specific gravity (g/cm ³)	3.11
Al ₂ O ₃	4.5	0.2	1.6	Initial setting time (min)	160
Fe ₂ O ₃	2.7	0.1	0.4	Final setting time (min)	240
CaO	63.0	0.4	46.3	Volume expansion (mm)	0.0
MgO	1.9	0.1	0.3	Specific surface Blaine (cm ² /g)	3811
SO ₃	3.1	0.1	0.1	Compressive Strength (MPa)	
K ₂ O	0.9	0.4	0.2	1 days	14.32
Ti ₂ O ₅	0.2	0.0	0.1	7 days	50.50
P ₂ O ₅	0.1	0.0	0.0	14 days	55.28
LOI	3.2	2.4	47.5	28 days	59.25
Na ₂ O	0.3	0.2	0.1		
Cl ⁻	0.1	0.0	0.0		

Limestone was ground until the required degree of fineness was achieved. The three materials produced from the same limestone, but of widely different fineness, were obtained and coded as 10 (8001 cm²/g), 20 (25,857 cm²/g), and 50 (25,954 cm²/g). Determination of the fineness and the specific surface area was performed with the air permeability method

(Blaine), according to the European standard EN 196-6. Grinding time was 10, 20, or 50 min, respectively. Limestones 20 and 50 had similar fineness [17].

Table 2. Coarse silica fume (H) with limestone (L) and cement (CEM I 42.5 R) mixes.

Cement Mix	Cement (%)	Coarse silica Fume (%)	Limestone Total (%)	10% Retained Limestone (%) (8001 cm ² /g)	20% Retained Limestone (%) (25,857 cm ² /g)	50% Retained Limestone (%) (25,954 cm ² /g)
Reference	100	0	0	0	0	0
H3L0-0-0	97		0	0	0	0
H3L10-0-0	87		10	10	0	0
H3L10-5-5	77		20	10	5	5
H3L15-0-0	82	3	15	15	0	0
H3L15-5-5	72		25	15	5	5
H3L20-0-0	77		20	20	0	0
H3L20-5-5	67		30	20	5	5
H5L5-0-0	95		0	0	0	0
H5-10-0-0	85		10	10	0	0
H5L10-5-5	75		20	10	5	5
H5L15-0-0	80	5	15	15	0	0
H5L15-5-5	70		25	15	5	5
H5L20-0-0	75		20	20	0	0
H5L20-5-5	65		30	20	5	5
H7L0-0-0	93		0	0	0	0
H7L10-0-0	83		10	10	0	0
H7L10-5-5	73		20	10	5	5
H7L15-0-0	78	7	15	15	0	0
H7L15-5-5	68		25	15	5	5
H7L20-0-0	73		20	20	0	0
H7L20-5-5	63		30	20	5	5

These new cements were used to make mortars with a cement-to-sand ratio of 1:3 and a water-to-cement ratio of 0.5 with distilled water and CEN standard sand [24]. The procedure of mortar mixing, molding, and curing is detailed in the European standard EN 196-1:2018 [24].

There were 3 mortar prisms made for each testing time: 7 and 28 days. The test specimens were 4 cm × 4 cm × 16 cm prisms. Test specimens were examined using a backscattered electron microscope (BEM) model S-4800 from Hitachi, Tokyo, Japan, and the components of mortars at 7 and 28 days were quantified using an X-ray dispersive energy microanalysis detector.

Testing

Water demand for normal consistency, initial setting time, and final setting time of cement paste were determined according to the European standard EN 196-3:2017 [25].

The chemical analyses were performed by XRF with an S8 Tigger 4 kW model instrument (Bruker, Billerica, MA, USA). Loss on ignition (LOI) and chloride ion contents were determined according to the European standard EN 196-2 [26].

The XRD test was performed using a D8 Advance powder crystal X-ray diffractometer (Bruker) with a 2.2 KW Cu anode ceramic X-ray tube.

Crystalline compounds were identified with the DIF-FRAC.EVA v4.2.1 software, Bruker Corporation headquarters in Billerica, MA, USA, which supports a reference pattern database, derived from the Crystallography Open Database (COD), for phase identification. The crystalline phases are measured using Rietveld refinement with an internal standard of α -Al₂O₃.

Mortar prisms were sectioned using a water-cooled diamond saw to retrieve mortar samples. Later, sample sections were further reduced in size, for examination by scanning electron microscopy (SEM), using backscattered electron imaging contrast and a low-speed

saw with propanol lubricant to produce approximately $10 \times 10 \times 10 \text{ mm}^3$ mortar specimens. Then, they were impregnated with a low-viscosity epoxy using a vacuum system, as well as polished, sputter-coated with carbon, and examined using an Electron Microscope (S-4800 from Hitachi) equipped with an X-ray detector by EDX, energy dispersive X-ray spectrometer (XFlash 5030 with Quantax microanalysis systems, Bruker Corporation headquarters in Billerica, MA, USA).

3. Results

3.1. Setting Time of Cement Mixtures

Following the procedures provided in the UNE-EN 196-3:2017 [25] standard, it is proposed to analyze several aspects of mixed cements, such as normal consistency and setting time. The consistency of the water used to create cement paste specimens is that of a regular consistency cement paste. Normal consistency cement paste is resistant to standard probe penetration. The amount of water necessary for said paste to penetrate is determined by performing serial penetration tests on pastes with varying water contents. Setting time is calculated by observing the penetration of a needle into a regular consistency cement paste until it reaches a predetermined value. The setting time was recorded in minutes.

Figure 1 depicts the setting time of cement mixtures. Maximum initial setting time was attained as 180 min at 3% of silica fume. This setting time is much greater than the initial setting time calculated for cement reference. Setting times decrease as the silica fume content increases. In the case of cements containing 7% silica fume, setting time values are even lower than those of the reference cement. In general, lower setting times than the reference cement, without any addition, are found. The prolonged setting time of cement paste depends upon the proportion of silica fume and limestone, as well as the type of cement.

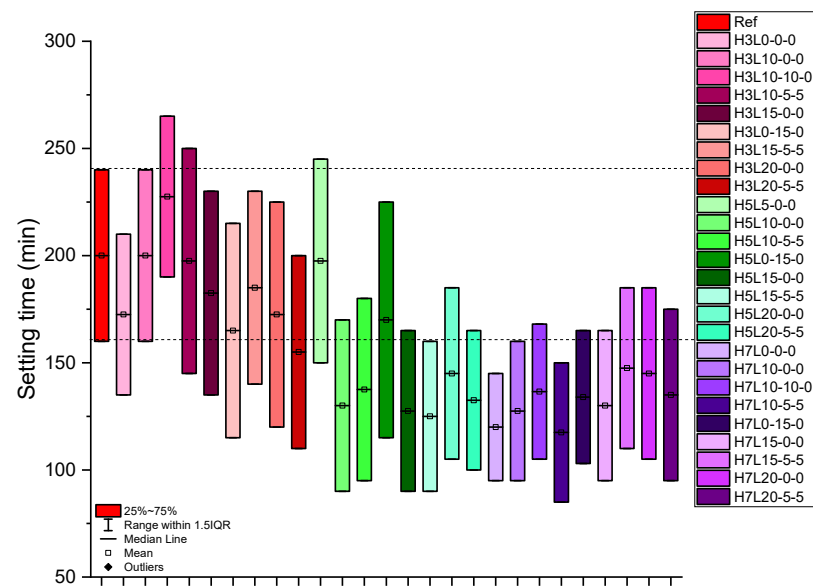


Figure 1. Setting time of cement mixtures.

3.2. X-ray Diffraction of Cement Paste Mixture

The development of the cement paste's crystalline phases at ages 1, 7, 14, and 28 days is studied. Rietveld refining, using an internal standard of alpha-corundum, provides the composition of the crystalline phases. X-ray diffraction can be used to measure the phases over time. The evolution of the crystalline phases of the reference cement is studied first, followed by the samples H3L5-0-0 and H7L15-0-0, in which the coarse silica fume content varies, and the evolution of the crystalline phases is not determined in any sample with 5% coarse silica fume because there are no significant differences in terms of physical properties. The development of the portlandite at different ages of the reference cement

(a), the H3L15-0-0 cement (b), and the H7L15-0-0 cement is shown in Figure 2. Then, the Portlandite crystallographic change of the reference cement, over time, is shown in Figure 2, whereas Figure 3 shows the crystalline phases in the reference cement.

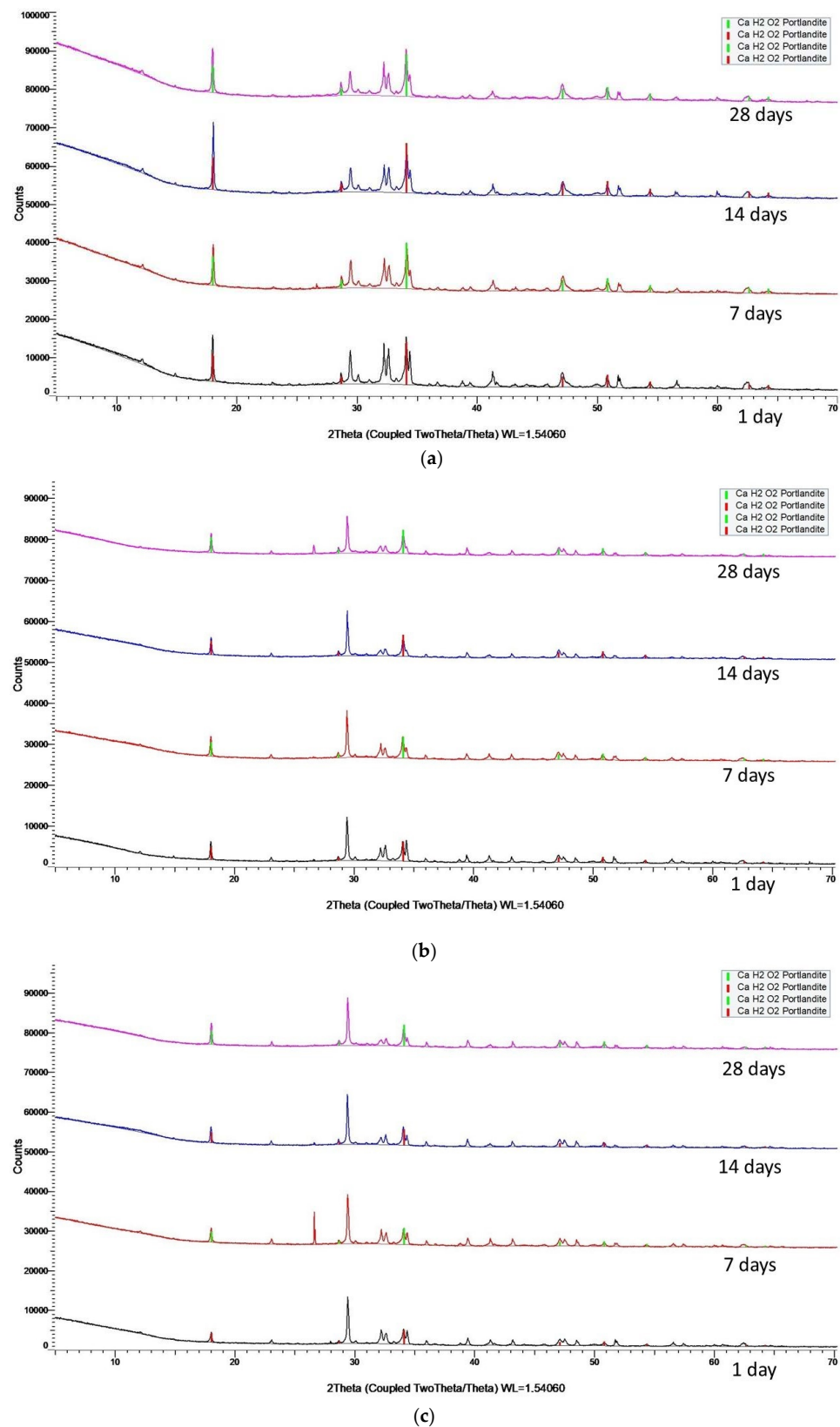
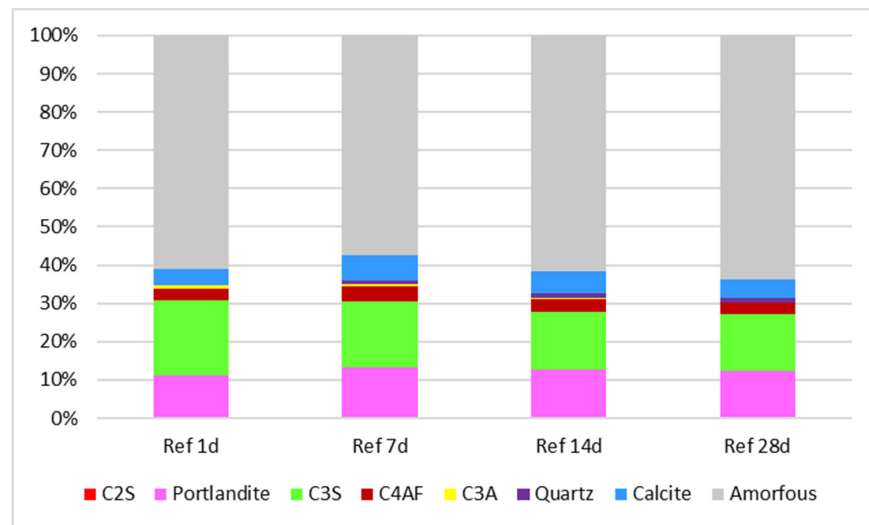
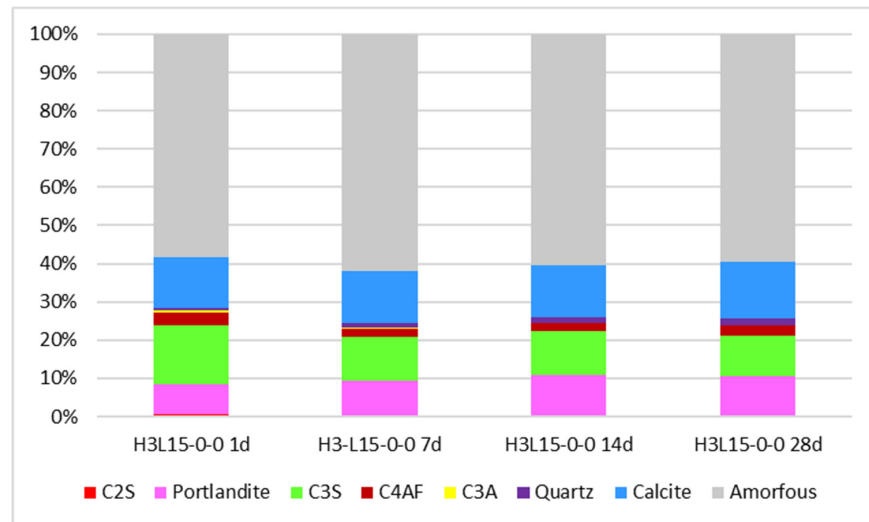


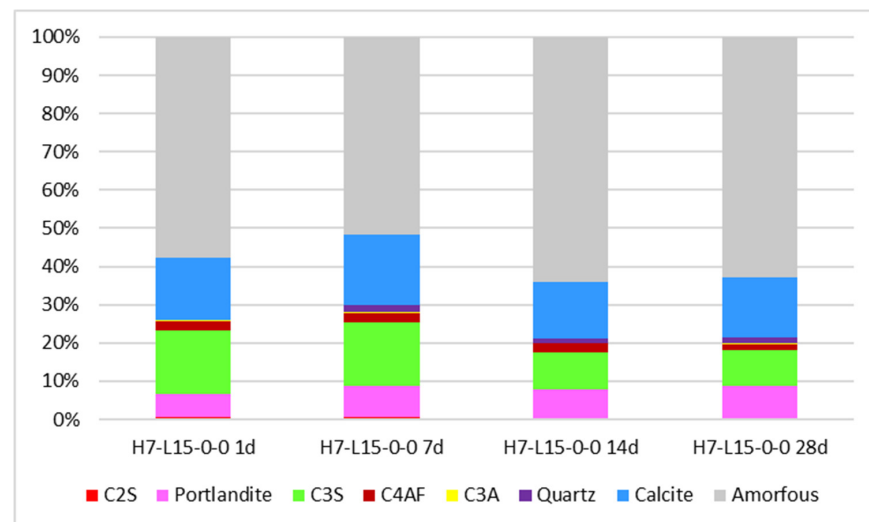
Figure 2. Portlandite crystallographic change, over time, of the reference cement (a), H3L15-0-0 (b), and H7L15-0-0 (c).



(a)



(b)



(c)

Figure 3. The quantification of the crystalline phases in the reference cement (a), H3L15-0-0 (b), and H7L15-0-0 (c) by X-ray diffraction.

Regarding the cements' mineralogical compositions, the diffraction spectra do not reveal any appreciable changes between them.

On the other hand, Figure 3 shows the time evolution of the quantified crystallographic phases, demonstrating that the portlandite increases as the hydration reaction progresses in the case of the reference cement (Ref). In the rest of the cements, this behavior is not observed because part of the portlandite is consumed to produce hydrated calcium silicate gels through the pozzolanic reaction.

As the hydration reaction develops, the amorphous content of the cement increases, and the anhydrous content decreases. This behavior is accelerated in the case of cements with pozzolanic components because they include a larger content of amorphous phases that can be related to higher quantities of C-S-H gels, which results in materials produced with these combinations having predictably better mechanical behavior.

3.3. Microstrural Characteristics

Figure 4 shows scanning electron microscopy (SEM) microphotographs of coarse silica fume (a) and limestone (b), whereas Figure 5 shows the back-scattered electron (BSE) micrographs of mortars either at 7 days or 28 days. The refining of pores by the addition of silica fume is often attributed to two effects. The first is the filling effect. It is broadly stated in the literature that silica dioxide nanoparticles fill the pores in the cement binder and contribute to forming a denser concrete structure [27–29]. Mukharjee and Barai [27] used the backscattered-mode scanning electron microscopic analysis to characterize the interfacial transition zone (ITZ) of concrete mixes and found the improvement of the microstructure of concrete mixes by adding silica fume. In addition, Frýbort et al. [29] confirmed the preventive effect of silica fume on preventing the expansion reactions in concrete. After 18 years of testing, no expansive silica gels were found. The morphology of silica fumes is normally spherical and can range from 20 nm to 500 nm. Zhoua et al. [30], by the use of scanning electron microscope (SEM) images and transmission electron microscope (TEM) images, studied a series of mesoporous silica fabricated by using silica fume. They presented the possibility of finding different sizes of this material. A coarse silica fume can be considered in the case of the material being studied [30].

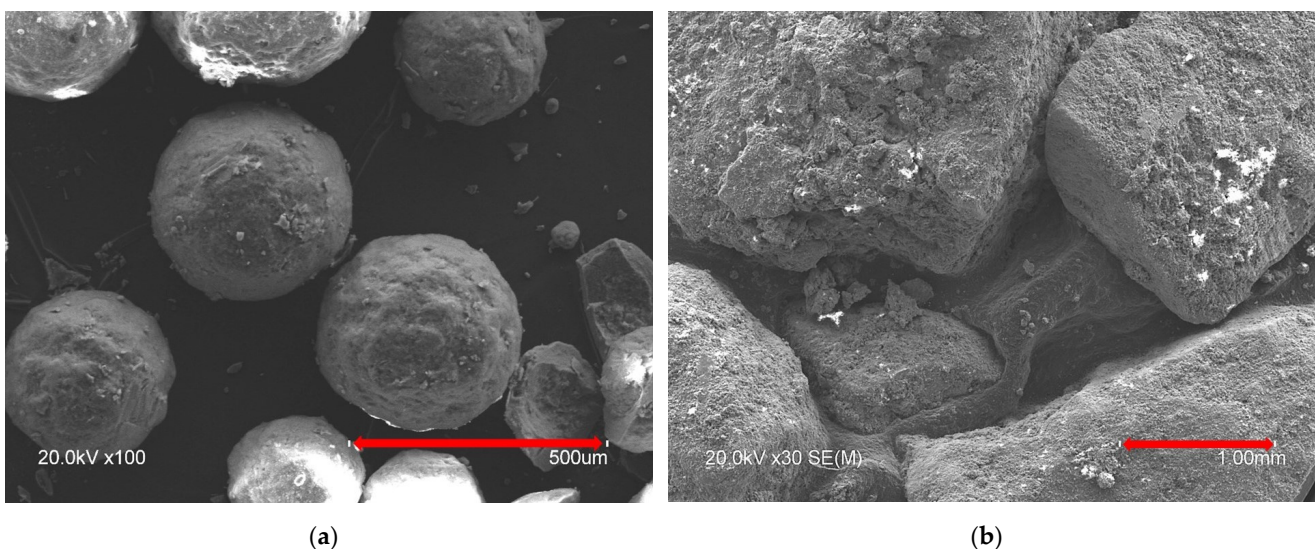


Figure 4. Scanning electron microscopy (SEM) microphotographs: (a) coarse silica fume; (b) limestone.

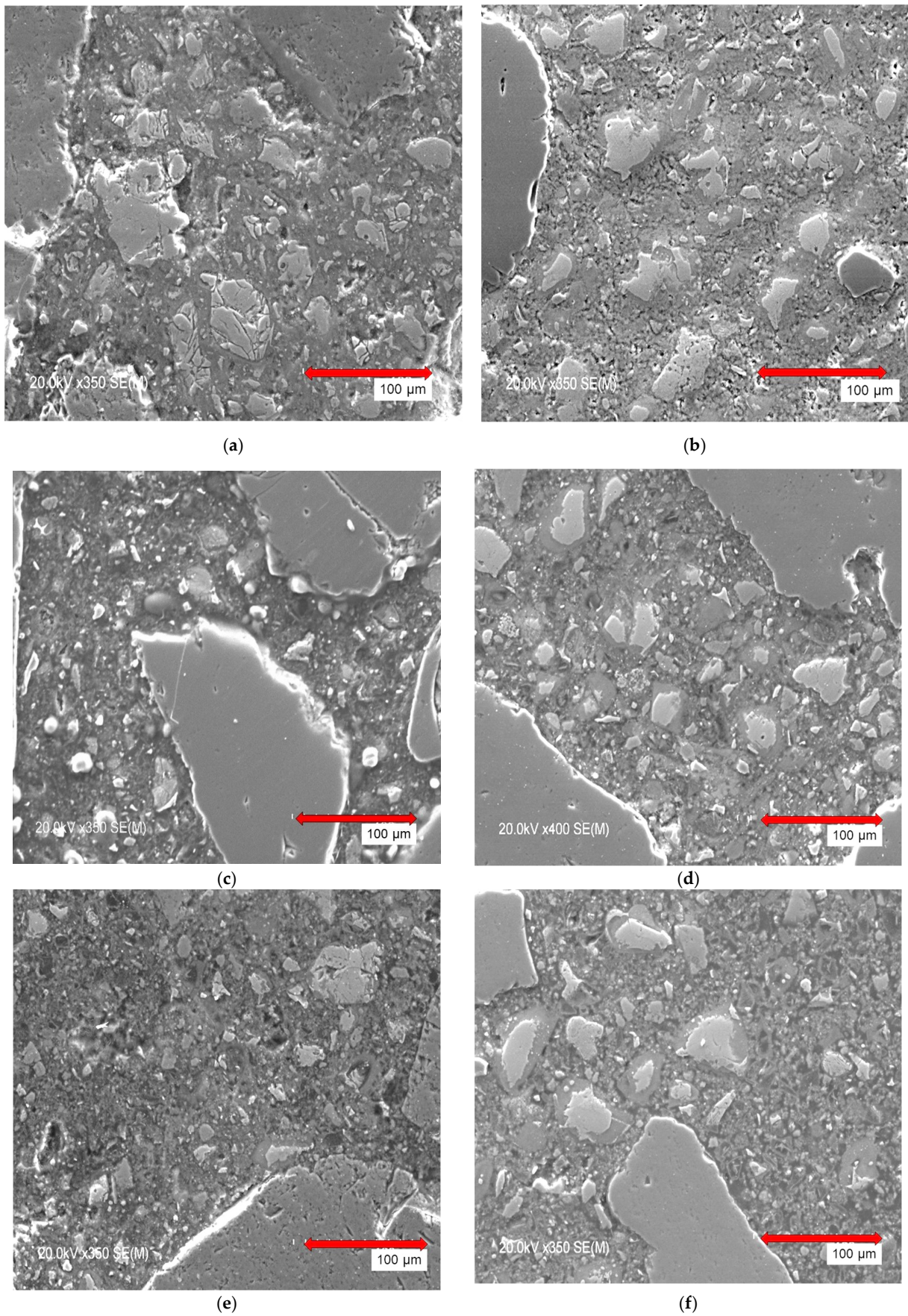


Figure 5. Cont.

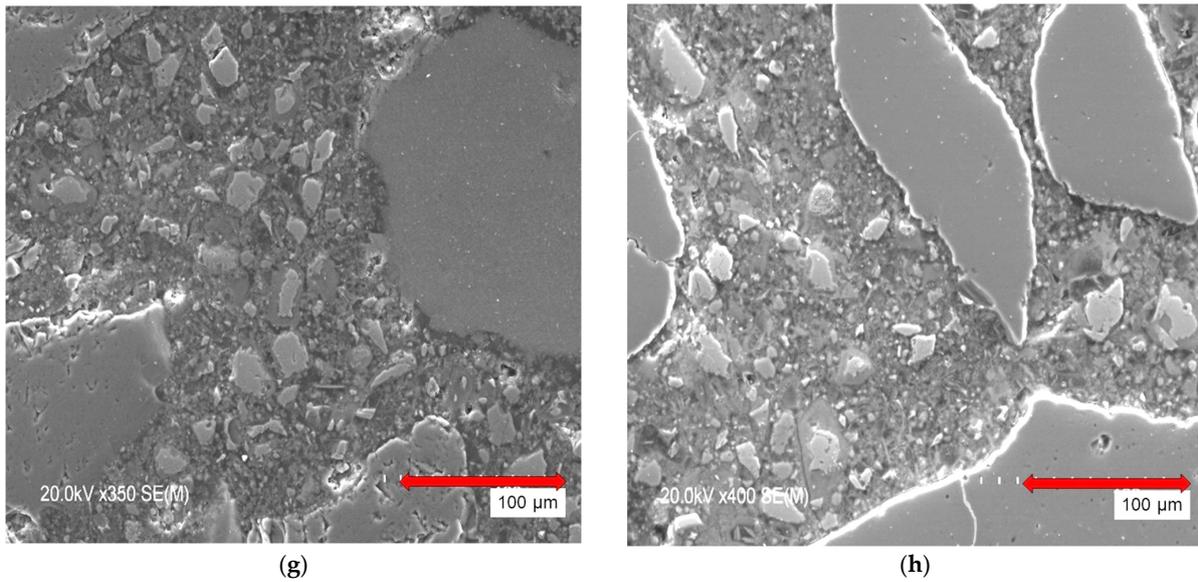


Figure 5. Back-scattered electron (BSE) micrographs of mortars either at 7 days or 28 days: (a) CEM I (Ref) 7 days; (b) CEM I (Ref) 28 days; (c) H3L15-0-0 7 days; (d) H3L15-0-0 28 days; (e) H5L15-0-0 7 days; (f) H5L15-0-0 28 days; (g) H7L15-0-0 7 days; (h) H7L15-0-0 28 days.

Limestone has angular particles and a porous texture (Figure 4b); the size of the limestone normally ranges between sand and gravel particles.

The evolution of the paste composition, over time, was tested in mortar specimens at different hydration ages and different contents in coarse silica fume. A gradual decrease in size of the anhydrous phases was observed along the time (Figure 6). This finding was more evident in mortars containing 5% of silica fume. Through the pozzolanic reactions, coarse silica fume combined with calcium hydroxide, providing a denser microstructure and rendering free lime unavailable for acid or sulphates attacks [31]. Kwon et al. reported that specimens incorporating silica fume showed a denser microstructure, which is explained by the pore filling effect [32].

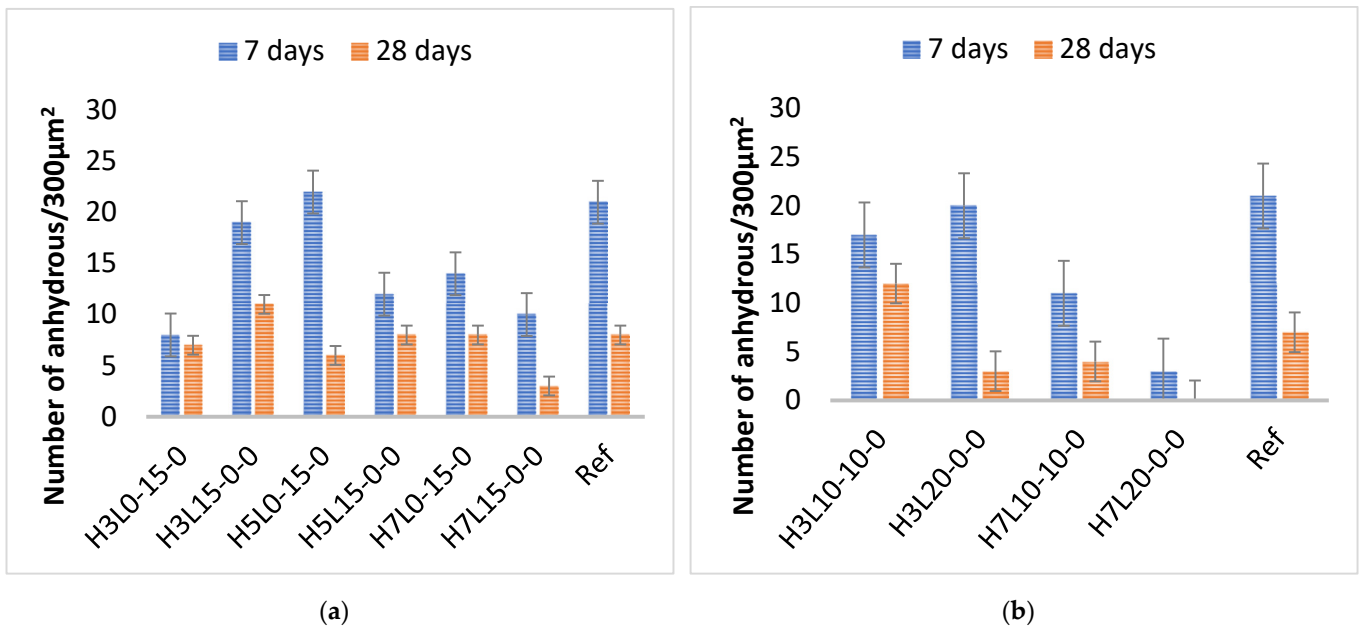


Figure 6. Number of anhydrous of mortars with (a) 15% and (b) 20% of limestone.

The incorporation of silica fume in cement is commonly known to reduce cracking caused by the aggregate–alkali reaction, particularly in the case of extremely reactive aggregates [33]. Coarse silica fume works as a source of amorphous silica in the case study, perhaps contributing to the development of ASR.

The mortars without additions showed a homogeneous paste with some anhydrous cement particles in white—(a) and (b)—that decrease as the specimen age increases; however, in the sample H3L15-0-0, we can discern anhydrous cenospheres (c) and (d). There do not appear to be any significant changes in the microstructure of the samples H5L15-0-0 (e) and (f) and H7L15-0-0 (g) and (h).

The Analysis Image Processing Analysis Docu program is used to calculate both the number and average size of the anhydrous cenospheres. Figure 6 quantifies the anhydrous content.

As the hydration phase progresses, the amount of cement anhydrous content decreases clearly, which is a behavior that accelerates as the silica fume content increases. On the other hand, it is clear that the addition of limestone filler to the cement and the decrease in the amount of anhydrous cement are related. The hydration process and setting behavior of Portland cement clinker are affected by the addition of CaCO_3 and CaSO_4 . Limestone has a beneficial effect on the technical qualities of cement and concrete when added in tiny amounts. The filler effect was used to describe how limestone improved the characteristics of cement. Calcite has also been revealed to be a reactive cement component by more recent studies [34–36].

According to Zajac et al. [36], small content of calcite leads to the hemicarbonates and monocarbonates formation, as well as more ettringite, in Portland cement. Hemicarbonates generation is kinetically favored. However, it is thermodynamically less stable than monocarbonates formation.

Kakali et al. [34] studied the effect of the presence of calcium carbonate on the C_3A and C_3S hydration. They found that the transformation of ettringite to monosulfate was delayed. In addition, monocarbonate was preferably produced instead of monosulfate. Finally, C_3S hydration was accelerated.

A comparative analysis of the paste composition at 7 and 28 days, for several samples, is shown in Figure 7. The chemical composition was determined by using an energy-dispersive X-ray spectroscopy (EDX) system based on a Hitachi scanning electron microscope (Bruker). The paste composition is adjusted to express the Al, Ca, and Si normalized atomic percentage, in a triangular pattern, at 7 days (Figure 7a) and 28 days (Figure 7b).

The chemical composition of silica fume varies depending on the manufacturing process; however, vitreous cenospheres are typically created with a silicon richness of more than 98% of their mass. In general, cements created with silica fume include a significant amount of silicon, and because this product is hydraulically active, it partially consumes the portlandite reserves to generate hydrated calcium silicate gels [37].

The Si/Ca ratio can be plotted against the Al/Ca ratio to track the evolution of alkaline reserves (Portlandite) over time. Figure 8 shows the time variation at 7 days (a) and 28 days (b).

Through the analysis of data, it has been discovered that portlandite (CH), which is produced after the hydration of Portland cement clinker, degrades over time. This process is caused by the pozzolanic reaction of microscopic silica silicates, which react with portlandite to produce hydrated calcium silicates (CSH), which increase the material's mechanical resistance while decreasing porosity and densifying the paste. This procedure also reduces the material's alkaline reserve, making this kind of mix potentially more vulnerable to acid attack and resulting in a decrease in pH. On the other hand, considering that the Si/Ca ratio does not change over time in comparison to the Al/Ca ratio, in the case of the reference, the portlandite has no degradation over time because there are no pozzolanic components in this mixture.

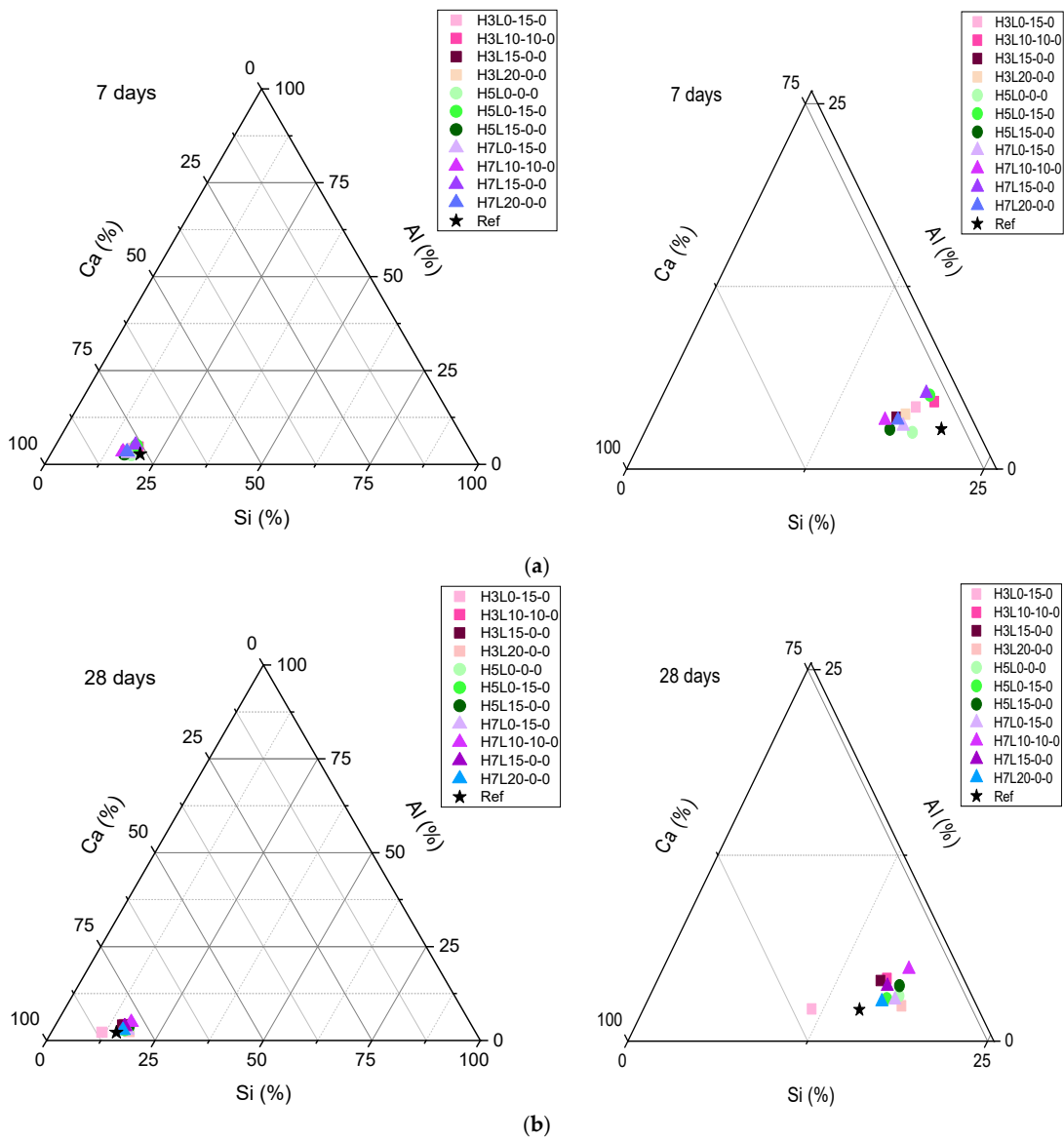


Figure 7. Energy-dispersive X-ray spectroscopy (EDX) paste composition: (a) 7 days; (b) 28 days.

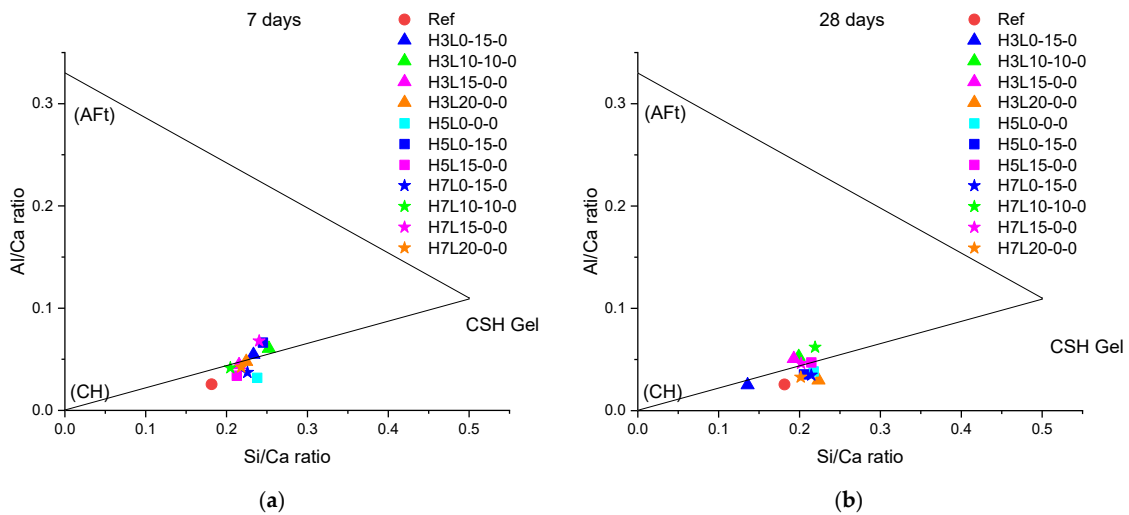


Figure 8. Si/Ca ratio versus Al/Ca ratio: (a) 7 days; (b) 28 days.

4. Discussion

In general, setting periods for cements containing 3% coarse silica fume are comparable to those for the reference cement. The results are clearly dispersed in the remaining mixtures, which may be caused by the silica fume's thickness and the varying fineness of the limestones used as filler to the ternary cements. As seen at the crystallographic level, a portion of the portlandite (CH) produced by the hydration reaction of the clinker components reacts with amorphous silica in coarse silica fume to produce hydrated calcium silicates, C–S–H gel, so it is important to note that the setting times decrease significantly as the coarse silica fume content increases. The nucleation of the clinker components, brought on by the limestone filler added to the cement, facilitates this pozzolanic reaction.

Microstructural analysis, on the other hand, concludes that, as the hydration reaction of the cement develops, more densified and less porous pastes are observed in cements containing higher amounts of coarse silica fume. Furthermore, an increase in the normalized atomic percentage of Silicon (Si) and Calcium (Ca) is detected in all microanalysis pastes, especially in combinations with pozzolanic additives. This phenomenon has the ability to increase the paste's Si/Ca ratio, which is a sign of how the pozzolanic reaction is progressing. In addition, a reduction in the quantity of anhydrous particles is seen in all situations; this behavior is more pronounced in mixes that contain more limestone filler.

This interaction makes it evident that, depending on its chemical composition and fineness, adding limestone filler as an inert material does not match the empirical evidence. In addition to reducing the carbon footprint produced by the decarbonization of raw materials during the manufacturing process of Portland cement clinker, this material has the potential to improve ternary cements.

5. Conclusions

The combined effect of silica fume and limestone addition affects the hydration process and setting time development. Silica fume and limestone can both be inactive and active components. The ratio of their action varies based on both their individual composition and the time of hydration.

Setting times decrease as the silica fume content increases. Furthermore, silica fume is responsible of pore size refinement in the cement paste by means of two effects, i.e., filling effect and pozzolanic reaction. Consequently, a denser microstructure has been found in silica fume cement pastes. As expected, a gradual decrease in size of the anhydrous phases was observed over time. Nevertheless, this finding was more evident in mortars containing 5% of silica fume.

Portlandite increases as the hydration reaction progresses in the case of the reference cement. By contrast, the portlandite is consumed by silica fume cements to produce hydrated calcium silicate gels through the pozzolanic reaction. As the hydration reaction develops, the amorphous content of the cement increases, and the anhydrous content decreases. This fact is accelerated in the case of cements with pozzolanic constituents, i.e., a higher content of C–S–H gel was found.

Higher quantities of amorphous phases are determined, as the materials age, by studying the hydration responses of the cements. Furthermore, it is clear that the pozzolanic components consume a portion of the portlandite to produce C–S–H gels, providing mechanical resistance to the material. This phenomenon can easily deplete the alkaline reserve of the porous network of the concrete; thus, it must be considered, especially, in structures produced with steel reinforcement that are susceptible to corrosion or at risk of significant exposure to chlorides.

Author Contributions: Conceptualization, E.M., H.R. and M.Á.S.; methodology, E.M., H.R. and M.Á.S.; validation, E.M. and H.R.; investigation, E.M., H.R. and M.Á.S.; resources, E.M.; data curation, E.M., H.R. and M.Á.S.; writing—original draft preparation, E.M., H.R. and M.Á.S.; writing—review and editing, E.M., H.R. and M.Á.S.; formal analysis, H.R. and M.Á.S. All authors have read and agreed to the published version of the manuscript.

Funding: This research was funded by the CSIC (PIE 202060E176).

Data Availability Statement: Not applicable.

Acknowledgments: Authors gratefully acknowledge the valuable contributions of Beatriz Aldea, Esther Puerto and Carmen Barba.

Conflicts of Interest: The authors declare no conflict of interest.

References

1. Council of the European Union. *Communication from the Commission to the European Parliament, the Council, the European Economic and Social Committee and the Committee of the Regions. 'Fit for 55': Delivering the EU's 2030 Climate Target on the Way to Climate Neutrality. COM/2021/550 Final*; Council of the European Union: Brussels, Belgium, 14 July 2021; Available online: <https://eur-lex.europa.eu/legal-content/EN/TXT/PDF/?uri=CELEX:52021DC0550&from=EN> (accessed on 5 July 2023).
2. European Commission, European Union. *A New Industrial Strategy for Europe. Communication from the Commission to the European Parliament, the European Council, the Council, the European Economic and Social Committee and the Committee of the Regions*; 10th of March 2020 COM (2020) 102 Final; European Commission: Brussels, Belgium, 2020; Available online: https://ec.europa.eu/info/sites/info/files/communication-eu-industrial-strategy-march-2020_en.pdf (accessed on 5 July 2023).
3. Sanjuán, M.A.; Argiz, C.; Mora, P.; Zaragoza, A. Carbon Dioxide Uptake in the Roadmap 2050 of the Spanish Cement Industry. *Energies* **2020**, *13*, 3452. [[CrossRef](#)]
4. Frías, M.; Monasterio, M.; Moreno-Juez, J. Physical and Mechanical Behavior of New Ternary and Hybrid Eco-Cements Made from Construction and Demolition Waste. *Materials* **2023**, *16*, 3093. [[CrossRef](#)] [[PubMed](#)]
5. Agrela, F.; Alaejos, P.; Thomas, C.; Rueda, J.; Silva, R.V.; Moreno, J.; Sanjuán, M.A.; de Brito, J.; Sánchez de Rojas, M.I. Normative review and necessary advances to promote the use of recycled aggregates and by-products in cement-based materials. In *Waste and Byproducts in Cement Based Materials*; Elsevier: Amsterdam, The Netherlands, 2021; pp. 735–776.
6. Zeraoui, A.; Maherzi, W.; Benzerzour, M.; Abriak, N.E.; Aouad, G. Development of Flash-Calcined Sediment and Blast Furnace Slag Ternary Binders. *Buildings* **2023**, *13*, 333. [[CrossRef](#)]
7. Pinheiro, D.G.L.; Sousa, M.I.C.; Pelisser, F.; da Silva Rêgo, J.H.; Moragues Terrades, A.; Frías Rojas, M. Physical and Chemical Effects in Blended Cement Pastes Elaborated with Calcined Clay and Nanosilica. *Materials* **2023**, *16*, 1837. [[CrossRef](#)]
8. Papatzani, S.; Paine, K. A Step by Step Methodology for Building Sustainable Cementitious Matrices. *Appl. Sci.* **2020**, *10*, 2955. [[CrossRef](#)]
9. Li, P.; Wang, X.; Cao, H. Empirical Compression Model of Ultra-High-Performance Concrete Considering the Effect of Cement Hydration on Particle Packing Characteristics. *Materials* **2023**, *16*, 4585. [[CrossRef](#)]
10. Zhao, Y.; Dong, X.; Zhou, Z.; Long, J.; Lu, G.; Lei, H. Investigation on Roles of Packing Density and Water Film Thickness in Synergistic Effects of Slag and Silica Fume. *Materials* **2022**, *15*, 8978. [[CrossRef](#)]
11. Srinivas, D.; Dey, D.; Panda, B.; Sitharam, T.G. Printability, Thermal and Compressive Strength Properties of Cementitious Materials: A Comparative Study with Silica Fume and Limestone. *Materials* **2022**, *15*, 8607. [[CrossRef](#)]
12. Kang, S.-H.; Hong, S.-G.; Moon, J. Performance Comparison between Densified and Undensified Silica Fume in Ultra-High Performance Fiber-Reinforced Concrete. *Materials* **2020**, *13*, 3901. [[CrossRef](#)]
13. Li, P.P.; Brouwers, H.J.H.; Chen, W.; Yu, Q.L. Optimization and characterization of high-volume limestone powder in sustainable ultra-high performance concrete. *Constr. Build. Mater.* **2020**, *242*, 118112. [[CrossRef](#)]
14. Richard, P.; Cheyrezy, M. Composition of reactive powder concretes. *Cem. Concr. Res.* **1995**, *25*, 1501–1511. [[CrossRef](#)]
15. Sanjuán, M.Á.; Andrade, C. Reactive Powder Concrete: Durability and Applications. *Appl. Sci.* **2021**, *11*, 5629. [[CrossRef](#)]
16. Oertel, T.; Hutter, F.; Helbig, U.; SEXTL, G. Amorphous silica in ultra-high performance concrete: First hour of hydration. *Cem. Concr. Res.* **2014**, *58*, 131–142. [[CrossRef](#)]
17. Sanjuán, M.Á.; Menéndez, E.; Recino, H. Mechanical Performance of Portland Cement, Coarse Silica Fume, and Limestone (PC-SF-LS) Ternary Portland Cements. *Materials* **2022**, *15*, 2933. [[CrossRef](#)] [[PubMed](#)]
18. Bentz, D.P. Activation energies of high-volume fly ash ternary blends: Hydration and setting. *Cem. Concr. Compos.* **2014**, *53*, 214–223. [[CrossRef](#)]
19. Cao, M.; Ming, X.; He, K.; Li, L.; Shen, S. Effect of macro-, micro- and nano-calcium carbonate on properties of cementitious composites—A review. *Materials* **2019**, *12*, 781. [[CrossRef](#)] [[PubMed](#)]
20. Chen, J.J.; Kwan, A.K.H.; Ng, P.L.; Li, L.G. Packing density improvement through addition of limestone fines, superfine cement and condensed silica fume. *J. Mater. Sci. Chem. Eng.* **2016**, *4*, 29–36. [[CrossRef](#)]
21. Knop, Y.; Peled, A. Packing density modeling of blended cement with limestone having different particle sizes. *Constr. Build. Mater.* **2016**, *102*, 44–50. [[CrossRef](#)]
22. Dhandapani, Y.; Santhanam, M.; Kaladharan, G.; Ramanathan, S. Towards ternary binders involving limestone additions—A review. *Cem. Concr. Res.* **2021**, *143*, 106396. [[CrossRef](#)]
23. UNE EN 197-1; Cement—Part 1: Composition, Specifications and Conformity Criteria for Common Cements. European Standard. Spanish Association for Standardization (UNE): Madrid, Spain, 2011.

24. EN 196-1:2016; Methods of Testing Cement—Part 1: Determination of Strength. European Committee for Standardization (CEN): Brussels, Belgium, 2016.
25. EN 196-3:2017; Methods of Testing Cement—Part 3: Determination of Setting Times and Soundness. European Committee for Standardization (CEN): Brussels, Belgium, 2017.
26. EN 196-2:2014; Method of Testing Cement—Part 2: Chemical Analysis of Cement. European Committee for Standardization (CEN): Brussels, Belgium, 2014.
27. Bhusan Mukharjee, B.; Barai, S.V. Influence of Incorporation of Nano-Silica and Recycled Aggregates on Compressive Strength and Microstructure of Concrete. *Constr. Build. Mater.* **2014**, *71*, 570–578. [[CrossRef](#)]
28. Xu, J.; Kong, F.; Song, S.; Cao, Q.; Huang, T.; Cui, Y. Effect of Fenton Pre-Oxidation on Mobilization of Nutrients and Efficient Subsequent Bioremediation of Crude Oil-Contaminated Soil. *Chemosphere* **2017**, *180*, 1–10. [[CrossRef](#)] [[PubMed](#)]
29. Frýbort, A.; Janaštilířová, J.J.; Grošek, J.; Gregerová, M. Changes in the Chemical Composition of Silica Fume in the Concrete Composite System. *Case Stud. Constr. Mater.* **2023**, *18*, e01916. [[CrossRef](#)]
30. Zhou, C.; Yan, C.; Zhao, J.; Wang, H.; Zhou, Q.; Luo, W. Rapid Synthesis of Morphology-Controlled Mesoporous Silica Nanoparticles from Silica Fume. *J. Taiwan Inst. Chem. Eng.* **2016**, *62*, 307–312. [[CrossRef](#)]
31. Khan, K.; Amin, M.N.; Usman, M.; Imran, M.; Al-Faiad, M.A.; Shalabi, F.I. Effect of Fineness and Heat Treatment on the Pozzolanic Activity of Natural Volcanic Ash for Its Utilization as Supplementary Cementitious Materials. *Crystals* **2022**, *12*, 302. [[CrossRef](#)]
32. Kwon, Y.H.; Kang, S.H.; Hong, S.G.; Moon, J. Enhancement of Material Properties of Lime-Activated Slag Mortar from Intensified Pozzolanic Reaction and Pore Filling Effect. *Sustainability* **2018**, *10*, 4290. [[CrossRef](#)]
33. Juenger, M.C.G.; Ostertag, C.P. Alkali–Silica Reactivity of Large Silica Fume-Derived Particles. *Cem. Concr. Res.* **2004**, *34*, 1389–1402. [[CrossRef](#)]
34. Kakali, G.; Tsivilis, S.; Aggeli, E.; Bati, M. Hydration Products of C₃A, C₃S and Portland Cement in the Presence of CaCO₃. *Cem. Concr. Res.* **2000**, *30*, 1073–1077. [[CrossRef](#)]
35. Hawkins, P.; Tennis, P.D.; Detwiler, R.J.; Rachel, J. *The Use of Limestone in Portland Cement: A State-of-the-Art Review*; Portland Cement Association: Skokie, IL, USA, 2003; 36p.
36. Zajac, M.; Rossberg, A.; Le Saout, G.; Lothenbach, B. Influence of Limestone and Anhydrite on the Hydration of Portland Cements. *Cem. Concr. Compos.* **2014**, *46*, 99–108. [[CrossRef](#)]
37. Panjehpour, M.; Abdullah, A.; Ali, A.; Demirboga, R. A Review for Characterization of Silica Fume and Its Effects on Concrete Properties. *Int. J. Sustain. Constr. Eng. Technol.* **2011**, *2*, 2180–3242. Available online: <https://publisher.uthm.edu.my/ojs/index.php/IJSCET/article/view/343> (accessed on 7 June 2023).

Disclaimer/Publisher’s Note: The statements, opinions and data contained in all publications are solely those of the individual author(s) and contributor(s) and not of MDPI and/or the editor(s). MDPI and/or the editor(s) disclaim responsibility for any injury to people or property resulting from any ideas, methods, instructions or products referred to in the content.